Pergamon

Continental Shelf Research, Vol. 15, No. 4/5, pp. 451–473, 1995

0278–4343/95 $9.50 + 0.00

0278–4343(94)00056–5

Variability of currents in late spring in the northern Great South Channel*

CHANGSHENG CHEN,†‡ ROBERT C. BEARDSLEY† and RICHARD LIMEBURNER†

(*Received* 7 *June* 1993; *in revised form* 1 *March* 1994; *accepted* 15 *May* 1994)

Abstract—The residual flows computed from detided shipboard ADCP data collected in late spring 1988 and 1989 clearly show different circulation patterns in the near-surface and deeper regions in the Great South Channel (GSC). In the upper 50 m, the residual flow in the northern GSC consists of three principal currents: (1) a southward coastal current located along the western flank of the GSC; (2) a broad cyclonic circulation crudely following the local topography in the interior region of the northern GSC; and (3) a northeastward current along the western flank of Georges Bank. Below 50 m, the residual flow tends to be cyclonic along the local 100-m isobath in the northern GSC. These circulation patterns are consistent with the vertical distributions of water properties and the trajectories of satellite-tracked drifters drogued at 5 and 50 m. Comparisons with geostrophic current shears and numerical model results suggest that the residual flow in spring is driven primarily by tidal rectification over the shallower sides of the northern GSC and by buoyancy forcing over the deeper flanks of the GSC. The southward transports of low-salinity plume surface water and Maine Intermediate Water (MIW) were about 0.07 ± 0.03 Sv and 0.31 ± 0.38 Sv in April 1988 and about 0.12 ± 0.06 Sv and 0.66 ± 0.14 Sv in June 1989. The larger transports of low-salinity plume water and MIW found in June 1989 are believed to be due to the increased freshwater river discharge in 1989 and occurrence of a subsurface coastal jet current along the western flank of the GSC.

1. INTRODUCTION

EACH spring, almost the entire population of North Atlantic right whales migrates to the Great South Channel (GSC) region of the western Gulf of Maine (GOM), where unusually dense aggregations of the copepod *Calanus finmarchicus*, the primary food of the right whales, are found (CETAP, 1982). The South Channel Ocean Productivity EXperiment (SCOPEX) was conducted in late spring of 1988 and 1989 to identify and study the physical processes which help cause these dense zooplankton patches to form. Prior to this work, few direct current measurements had been made in the northern GSC region. Based on hydrographic and surface drifter observations, BIGELOW (1927) first suggested that the summertime surface circulation in the GOM is dominated by two relatively large-scale gyres: a cyclonic circulation around Jordan Basin and an anticyclonic circulation around Georges Bank. The surface circulation in the western GOM predicted in Bigelow's schematic is a combination of a cyclonic turning flow along the local isobaths in the

*Woods Hole Oceanographic Institution Contribution No. 8396.

†P.O. Department, Woods Hole Oceanographic Institution, Woods Hole, MA 02543, U.S.A.

‡Present Address: Department of Oceanography, Texas A&M University, College Station, TX 77843, U.S.A.

northern GSC, an anticyclonic recirculating flow around Georges Bank, and a southward current along the western flank of the GSC. GREENBERG (1983) used a barotropic primitive equation numerical model to examine the GOM residual flow due to rectification of the dominant semi-diurnal M_2 tidal component. He found anticyclonic flow around both Georges Bank and Nantucket Shoals and a weak (1–3 cm s^{-1}) mesoscale cyclonic recirculation cell (of order 30 km in diameter) in the northern GSC. Recent field work has demonstrated the importance of buoyancy forcing and tidal rectification in the seasonal circulation over Georges Bank (BUTMAN *et al.*, 1987; LODER *et al.*, 1992), however, little is actually known about the subtidal current field and its variability and driving mechanisms in the northern GSC.

CHEN *et al.* (1995) analyzed the 1988–1989 SCOPEX hydrographic data and found that the vertical structure of water properties in the upper 150 m in the northern GSC during spring is characterized by two distinct water masses, a low-salinity surface plume in the upper 40 m overlying a thick layer of relatively uniform Maine Intermediate Water (MIW). The *T–S* properties associated with these two water masses suggest that most of the deep MIW flows in a broad cyclonic current roughly along local isobaths in the northern GSC to join the anticyclonic circulation around Georges Bank, with little deep water exchange between the western GOM and the New England shelf through the GSC. The relatively strong horizontal density gradients found on the western side of the northern GSC between the low-salinity surface plume and offshore water imply that buoyancy forcing may be significant in the northern GSC in late spring.

The 1988–1989 SCOPEX field measurements showed that the area of highest zooplankton concentration was observed in the western GSC in 1988 and in the eastern GSC in 1989 (Fig. 1, upper panel). The same patterns were also exhibited by right whale sightings (Fig. 1, lower panel). Whether this spatial shift in zooplankton and right whale concentration is due to the temporal difference in the 1988 (April–May) and 1989 (May–June) experiments or interannual variability in other factors is not known. CHEN *et al.* (1995) presented evidence for a spring-time seasonal evolution in the water property structure in the northern GSC, especially in the formation and movement of the low-salinity surface plume. Both the plume and the deeper MIW may advect zooplankton and nutrients from the western GOM into the northern GSC in spring. When the southward-flowing, low-salinity surface plume meets nutrient-rich, vertically well-mixed shelf water flowing northward through the eastern GSC around Georges Bank, lateral mixing may lead to an increase of zooplankton in the GSC, and flow convergence may help maintain a persistent high concentration of large zooplankton there. Clearly, examination of these and other hypotheses concerning the role of advection in causing high zooplankton concentration in the northern GSC requires more information about the flow field in the GSC in late spring.

As part of SCOPEX, continuous Acoustic Doppler Current Profiler (ADCP) data were collected along the ship's track aboard the R.V. *Endeavor* using a 150-kHz RDI ADCP during three regional hydrographic surveys: 26–29 April 1988 (3 days), 19–22 May 1989 (4 days), and 6–12 June 1989 (6 days) (Fig. 2). ADCP data were also recorded for at least 20 hour-long periods at five stations along the 100-m isobath during several small-scale biological surveys during May–June 1989. The vertical resolution of the ADCP data was four meters, and the data were averaged over 5-min intervals. The relatively shallow depth of the northern GSC region allowed bottom tracking during the ADCP measurements so that high-quality absolute current profile data over the upper 140 m were obtained during

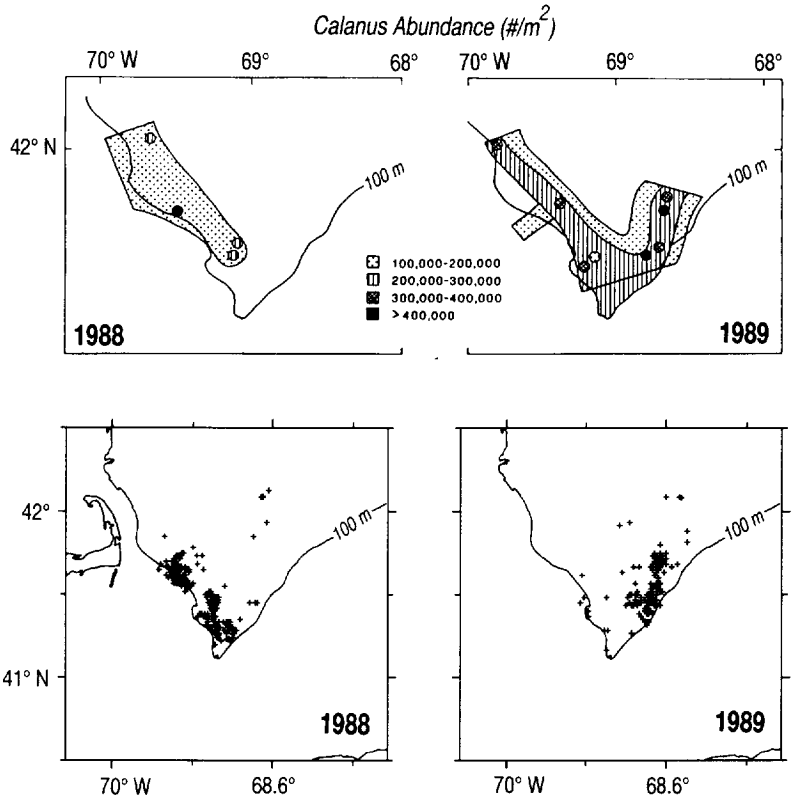

Fig. 1. Distributions of *Calanus* abundance (upper panel) and right whale sightings (lower panel) in the late spring of 1988 (left) and 1989 (right). Water column abundance (numbers m^{-2}) of total *Calanus* (copepodite 3 and older stages) is indicated by shading, with the key shown in the center of the upper panel. The symbols indicate locations of peak abundances. The maximum value in a day–night pair of abundance estimates at a site was used for contouring the abundance field. Individual whale sightings are shown as crosses in the lower panel. The upper panel is from WISHNER and SCHOENHERR (1992).

most of the April 1988 survey and all of the May–June 1989 surveys. However, instantaneous absolute currents obtained from the raw ADCP data in the northern GSC included strong semidiurnal tidal signals which were almost one order of magnitude larger than the residual flow. For this reason, an empirical least-squares method was used to remove the tidal currents from the raw ADCP current data. Good agreement between fitted and observed tidal currents allows us to use the ADCP data to describe the three-dimensional structure of the residual flow in the northern GSC in late spring, 1988 and 1989.

This paper is organized as follows. First, the analysis method used to detide the ADCP data is described. Second, the structure of the resulting residual currents is described. Third, the variability in the southward transport of the low-salinity surface plume and MIW in 1988 and 1989 is estimated based on the ADCP residual flow. Finally, conclusions are summarized.

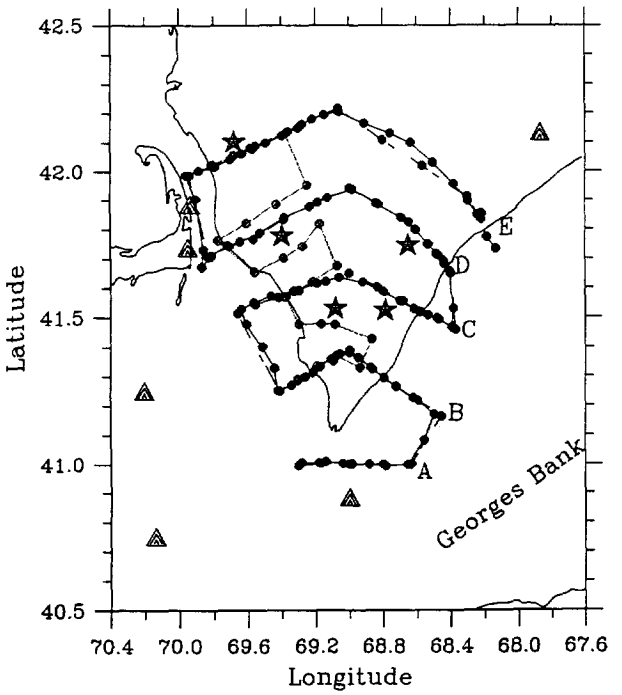

Fig. 2. Ship's tracks of the ADCP surveys taken along with regional SCOPEX CTD measurements during 26–29 April 1988 (dashed line), 18–21 May (solid line) and 6–12 June (heavy solid line) 1989. The roughly east–west transects during the April 1988 and June 1989 surveys are labelled from south to north as A through E. The stars represent the averaged position of small-scale ADCP surveys conducted in late May and early June 1989. The triangles represent positions where tidal data were available.

2. SEPARATING LOW-FREQUENCY AND TIDAL CURRENTS IN THE SCOPEX ADCP DATA

There are two primary concerns whenever ship-mounted ADCP data are used to study residual flow in the coastal ocean: (1) contamination from the ship's velocity and (2) contamination by tidal currents. In water depths less than 200-m, a 150-kHz RDI ADCP can directly track the bottom along the ship's course, and thus the ship's velocity can be determined from the bottom tracking velocity. Since the bottom tracking velocity is recorded in the same coordinates as the raw ADCP current profile data, the largest measurement errors in ship-mounted ADCP data are automatically cancelled once the bottom tracking velocity is subtracted from the current profile data, leaving only misalignment and sensitivity errors which can be made relatively small (of order less than 1 cm s^{-1}) with proper calibration (JOYCE, 1989; CHEN, 1989). On the other hand tidal currents are frequently much larger than the subtidal flow and may dominate the raw ADCP current data, making them useless for the study of residual flow. Removing the tidal currents from the raw ADCP data requires detailed information about the spatial and temporal structure of the tidal currents in the domain of study. Large fortnightly or longer term variability in the tidal currents may also exist in the raw ADCP data, possibly making it difficult to resolve each tidal component from a short ADCP measurement.

There has been no simple way available so far to filter tidal signals directly from the raw ADCP data recorded along a CTD survey track. The ship-mounted ADCP provides profiles of instantaneous current along the ship's track as a function of time and ship's position. If the ship is stationary over at least one tidal cycle, the ADCP data can be treated as a time series and then tidal signals can be easily filtered from the raw ADCP data using harmonic analysis or least-squares fit (GEYER and SIGNELL, 1990; LWISA and BOWERS, 1990; BEARDSLEY *et al.*, 1990). If the ship is moving, however, a different approach that allows for spatial variability of tidal currents must be used to separate tidal and residual currents from the raw ADCP data. One possible method to deal with this problem is to use a numerical model to predict the spatial and temporal structure of the tidal currents and then subtract them directly from the raw ADCP records (FREELAND and FOREMAN, 1990). However, this approach is constrained from its general application in most coastal regions due to the lack of good numerical tidal models. BEARDSLEY *et al.* (1990) treated ADCP data taken along a CTD tow-yo track within a small area about 5 × 5 km in the northern GSC as a time series and successfully used least-squares fitting to separate the tidal and residual currents there. CANDELA *et al.* (1992) recently extended the least-squares method to include a polynomial function to fit the spatial structure of tidal and subtidal currents observed in an ADCP survey. In the northern GSC, the cotidal and phase lines of the semi-diurnal and diurnal tides almost parallel the local isobaths (MOODY *et al.*, 1984). This simple tidal structure suggests that the tidal currents in the northern GSC may be removed from the SCOPEX ADCP data using the CANDELA *et al.* (1992) polynomial fitting method. Since this approach is quite new and was being developed during the course of this research, some modifications of this method have been made here to include the time variability of the fitted tidal currents due to the superposition of different tidal constituents during our surveys, and to resolve the vertical structure of the tidal and residual currents.

Without considering the non-linear interaction between tidal and subtidal currents, the total current field can be simply represented by

$$\vec{u} = \vec{u}_r + \sum_{n=1}^{K} (\vec{a}_n \cos \omega_n t + \vec{b}_n \sin \omega_n t), \tag{1}$$

where the index n denotes the semidiurnal and diurnal tidal components used in our fitting, $\vec{u}$ is the residual current vector, and $(\vec{a}_n, \vec{b}_n)$ are the amplitudes of the tidal components. CANDELA *et al.* (1992) succeeded in using first and second order polynomials as the empirical spatial functions of $\vec{u}_r$ and $(\vec{a}_n, \vec{b}_n)$, respectively, to fit the vertical integral transports of residual flow and semidiurnal (M_2) tidal currents in the northern East China Sea. In the northern GSC, however, the superposition of different tidal constituents (three semidiurnal tides M_2, N_2 and S_2 and two diurnal tides K_1 and O_1) makes a significant contribution to the temporal variability of the local tidal currents, even though the ratio of either N_2 or S_2 to M_2 for the equilibrium tide is only about 0.2 and the ratio of K_1 or O_1 to M_2 is less than 0.1 (MOODY *et al.*, 1984).

Two coastal tide stations and four bottom-pressure stations bracketing the northern GSC were chosen to investigate the fortnightly tidal modulation during these surveys (Fig. 2). A uniform spatial modulation was found in the tidal elevation during the April 1988 and May–June 1989 CTD/ADCP surveys. In June 1989, the amplitudes of S_2 and N_2 were of the same order, while their phase difference was about 180° at the beginning of the survey and then decreased with time during the survey. The combined contribution of these two

tidal constituents results in an approximately linear decrease of the amplitude of the total semidiurnal tide (a sum of M_2, S_2 and N_2) during the survey, but did not cause a frequency shift from M_2. In mid-May 1989, 3 weeks earlier, the amplitudes of S_2 and N_2 cancelled each other during most of the survey so that the total semidiurnal tidal component was equal to the M_2 tide except for a small phase shift. In contrast, a small phase difference was found between N_2 and S_2 at the beginning of the April 1988 survey; it became larger later, leading to an approximately linear increase of total semidiurnal tide with time during that survey. During all three surveys, the period of the total diurnal tide was equal to an average period of the K_1 and O_1 tides, and its amplitude was almost two times as large as either of these two tidal constituents. Since all stations exhibited the same temporal modulation, we expect the tidal elevation and currents within the study region to exhibit the same temporal variability.

Based on this assumption, we have chosen the M_2 frequency ($\omega_1 = 2\pi/12.4206$ h) and the mean frequency of K_1 and O_1 ($\omega_2 = 2\pi/24.8769$ h) as frequencies of the total semidiurnal and diurnal tidal components in our tidal fit for the SCOPEX ADCP data, and taken the combined contribution of N_2 and S_2 to the total semidiurnal tide into account by multiplying the amplitude of the fitted semidiurnal tidal current with a linearly time-dependent and spatially uniform correction term.* Therefore, the residual flow and the amplitude of tidal currents can be separately expressed by polynomial functions of the form

$$\vec{u}_r = \sum_{k=0}^{L} \sum_{i=0}^{k} \vec{u}_r l_{k+i} x^{k-i} y^i; \tag{2}$$

$$\begin{pmatrix} \vec{a}_1 \\ \vec{b}_1 \end{pmatrix} = \varepsilon \sum_{k=0}^{m_1} \sum_{i=1}^{k} \begin{pmatrix} \vec{a}_1 l_{k+i} \\ \vec{b}_1 l_{k+i} \end{pmatrix} x^{k-i} y^i; \tag{3}$$

$$\begin{pmatrix} \vec{a}_2 \\ \vec{b}_2 \end{pmatrix} = \sum_{k=0}^{m_2} \sum_{i=1}^{k} \begin{pmatrix} \vec{a}_2 l_{k+i} \\ \vec{b}_2 l_{k+i} \end{pmatrix} x^{k-i} y^i, \tag{4}$$

where L, m_1 and m_2 are degrees of the polynomial for the low-frequency, semidiurnal, and diurnal tidal currents, respectively. $l_{k+i} = \Sigma_i^k\, i$ is an integer which is equal to the total number of previous terms. ε is the linearly time-dependent correction factor for the semidiurnal tidal currents, given by

$$\varepsilon = \begin{cases} 1.2 - \dfrac{0.40}{t_N - t_0}(t - t_0) & \text{for the June 1989 survey,} \\ 1.0 & \text{for the May 1989 survey,} \\ 0.9 + \dfrac{0.18}{t_N - t_0}(t - t_0) & \text{for the April 1988 survey,} \end{cases}$$

where t_0 and t_N are the initial and final times of the survey.

*Note: This time-dependent correction for the semidiurnal tidal current is based on the assumption that the tidal current is proportional to the spatial gradient of tidal elevation. Of course, the effect of N_2 and S_2 tidal constituents on the total semidiurnal tidal current can be also taken into account by adding a time-dependent correction term into the amplitude of each fitted semidiurnal tidal current. This approach, however, must be done at the expense of reducing the degrees of freedom for the fitting function, possibly increasing the fitting within a given confidence level.

The multiple least-squares regression method used to fit the raw ADCP data is described in detail in the Appendix. Two statistical tests using the student's t-distribution and the F-distribution have been made to test if each coefficient in the regression equation is significantly different from zero at a 95% confidence level and if adding higher order polynomials into the regression gives a significantly better fit. The uncertainty in the predicted value from the true value at a fixed point is estimated using the standard deviation with a 95% confidence level (DRAPER and SMITH, 1966). The number of independent data samples is estimated from the ratio of the total time length of the ADCP data record to the de-correlation time scale of the continuous ADCP data. We found a de-correlation time scale of about 1 h for the residual currents for the 1988 and 1989 ADCP measurements, thus the raw ADCP data for all surveys were averaged into 1-h non-overlapping values along the ship's track to construct an independent data set for the residual flow analysis.

Direct fitting of the 1-h averaged ADCP current data using the empirical formulae (2)–(4) gave high correlations of 0.95 for u and 0.99 for v between the predicted and raw ADCP currents. Such high correlation may not be statistically meaningful for both tidal and residual currents because of the existence of narrow band tidal signals at semidiurnal and diurnal frequencies (CHELTON, 1982). For these reasons, two steps were taken to fit the tidal and residual flow in the SCOPEX 1-h averaged ADCP data. The first step was to find the best fit for the tidal currents using the empirical formulae with a low-order polynomial for the residual flow. The second step was to fit a "raw" residual current data series that was obtained by subtracting the model tidal currents found in step one from the original 1-h averaged ADCP currents. The uncertainty of model tidal currents was determined from the standard deviation of predicted tidal elevation obtained using the least squares method on the total observed elevation of semidiurnal and diurnal tides at the six reference tidal stations, while the errors in the model residual flow were calculated based on the measurement error and fitting uncertainty estimated from the least-square fit where the number of independent data samples is equal to the number of 1-h averaged data records. Good agreement between the predicted tidal currents and previous observations was found using this empirical least-squares approach. Since our focus here is on the residual flow, we will omit any further discussion of the tidal currents found in the northern GSC [interested readers can find a detailed description of this analysis method and the tidal currents deduced from the SCOPEX ADCP data in CHEN (1992)].

3. STRUCTURE OF RESIDUAL FLOW IN THE NORTHERN GSC

Structure of vertically averaged residual flow in the northern GSC

In principle, the vertically averaged residual flow* can be directly obtained by subtracting the fitted tidal currents from the vertically averaged ADCP currents since good tidal fitting implies little non-linear interaction between the tidal and subtidal currents.

*Note: The vertically averaged residual currents referred to here are the currents averaged over the whole water column where the ADCP data are recorded.

However, the residual flow so obtained may not provide a good snapshot of the Eulerian subtidal current field since the subtidal flow contains both temporal and spatial subtidal current variability and measurement noise. For this reason, we have taken the subtidal currents as a "raw" data set, and then refit it using the least-squares method. The *F*-test shows a best fit for the "raw" residual flow at a 95% confidence level with a second order polynomial, in which the correlation between the "raw" and fitted residual flow was found to be 0.60, 0.64 and 0.65 for u (east–west component) and 0.89, 0.91 and 0.93 for v (north–south component) for the April 1988 and May and June 1989 surveys, respectively. The standard deviation of the fitting for these three surveys was equal to 4.5, 2.2 and 3.7 cm s^{-1} for u and 6.5, 2.3 and 3.3 cm s^{-1} for v.

The vertically averaged residual flow in late spring during the April 1988 and May–June 1989 surveys is characterized by: (1) a cyclonic circulation in the central northern GSC region, (2) a southward coastal current east of Cape Cod over the western flank of the GSC, and (3) a northeastward flow along the western flank of Georges Bank (Figs 3–5). There were some differences in amplitude and direction of the residual current between the 1988 and 1989 surveys. In April 1988, the subtidal current was stronger and had a notable onshore component just east of Cape Cod, while in May and June 1989, the current was relatively weaker and tended to flow offshore along the local isobaths. The causes of this difference are not known, but may be partly due to a difference in the surface wind field between 1988 and 1989. The surface wind was stronger (>15 m s^{-1}) and southward for about two weeks before the April 1988 survey, but weaker (~5 m s^{-1}) and northward during the May and June 1989 surveys. This fact implies that the onshore transport during the April 1988 survey might have been driven by the southward downwelling-favorable wind stress while in turn the offshore transport in May and June 1989 might be due to the northward upwelling-favorable wind stress.

A notable temporal change in the residual current was found over the western flank of Georges Bank in late spring 1989. During 19–21 May 1989, although a relatively strong coastal current was beginning to enter the northern GSC region along the Cape Cod coast, the northeastward current over the western flank of Georges Bank was only about 1–2 cm s^{-1} (Fig. 4). About 3 weeks later during 7–12 June 1989, however, the northeastward flow on the western flank of Georges Bank was increased up to 7–8 cm s^{-1}, even though the magnitude of the southeastward coastal current over the western flank of the northern GSC remained almost unchanged (Fig. 5). This temporal variation was also found in the ADCP data from five small-scale biological surveys taken from 22 May to 4 June 1989. A weaker northeastward current of about 1.9 cm s^{-1} was found at Sta. 5 over the western flank of Georges Bank during 22–24 May 1989, quite similar to that measured during 7–19 May 1989 but about three times weaker than that found during the 7–12 June regional CTD/ADCP survey (see heavy arrows in Fig. 5). The intensification of the residual current over the western flank of Georges Bank may reflect the seasonal intensification of the anticyclonic circulation around Georges Bank described by BUTMAN *et al.* (1987).

The errors (with a 95% confidence limit) in the fitted residual current components vary along the ship's track. In April 1988, the fitting uncertainty ranged from ± 2.5 to ± 5.0 cm s^{-1} in u and ± 3.0 to ± 7.5 cm s^{-1} in v. In May 1989, the fitting uncertainty for the residual flow ranged from ± 1.0 to ± 2.5 cm s^{-1} for both u and v, while in June 1989, they were equal to ± 3.0–3.5 cm s^{-1} in u and ± 2.5–3.0 cm s^{-1} in v in the interior region of the ADCP survey area, but about ± 4.0 cm s^{-1} for both u and v just east of Cape Cod, in the southern GSC less than 70 m, and at the northeast corner of the survey area where the residual flow

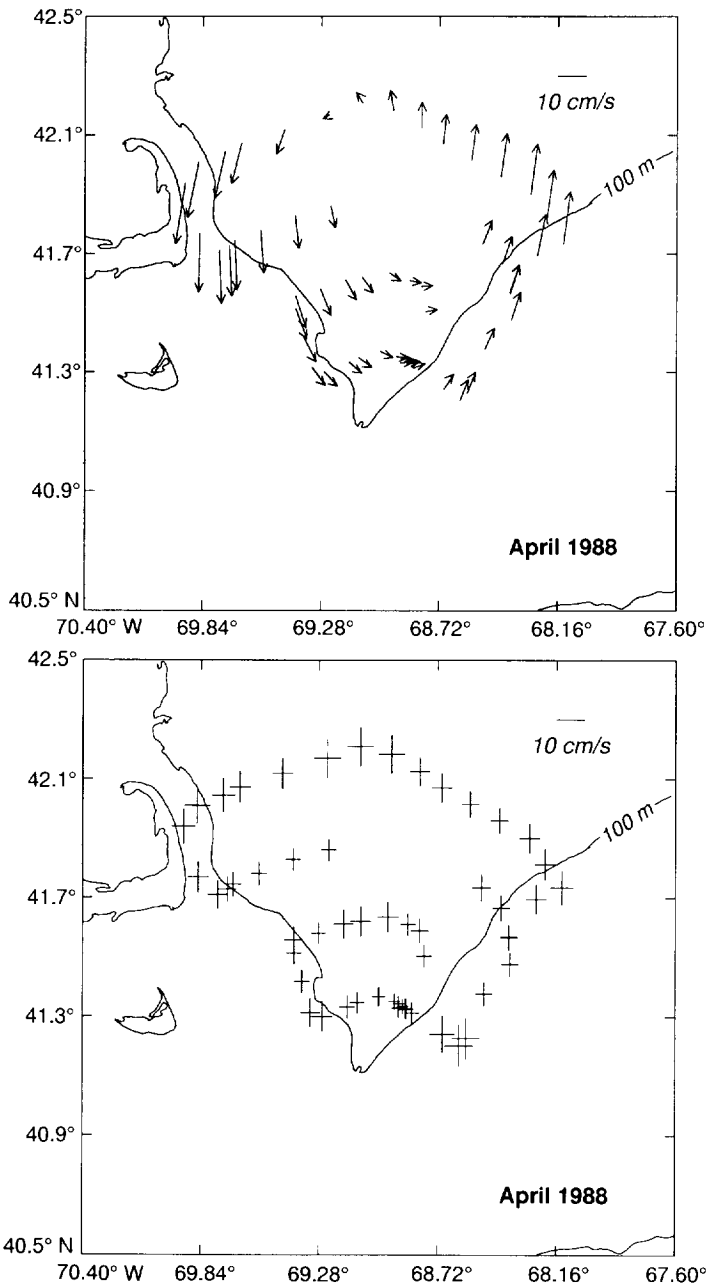

Fig. 3. Distributions of vertically averaged residual flow (upper) and fitting uncertainty (lower) in the northern GSC during the April 1988 CTD/ADCP survey. The plotting scale for the current vector and fitting uncertainty is shown in cm s^{-1} in the upper right of each panel.

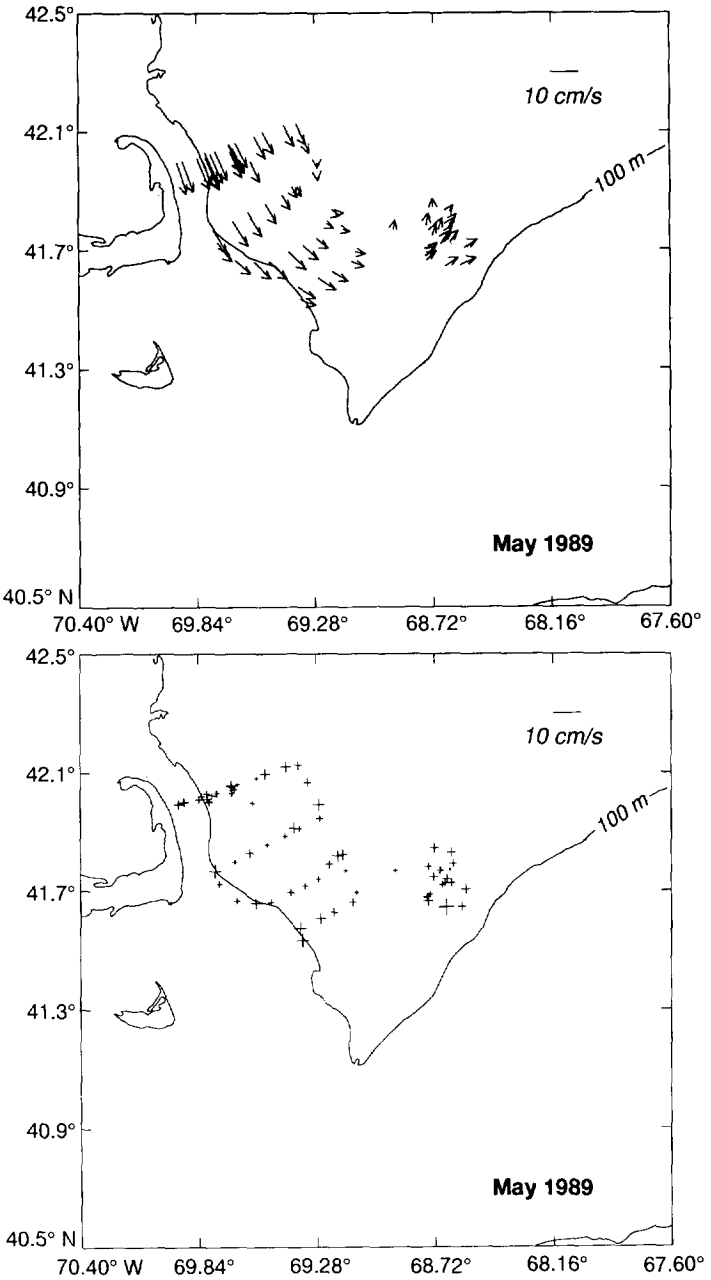

Fig. 4. Distributions of vertically averaged residual flow (upper) and fitting uncertainty (lower) in the northern GSC during the May 1989 CTD/ADCP survey. The plotting scale for the current vector and fitting uncertainty is shown in cm s^{-1} in the upper right of each panel.

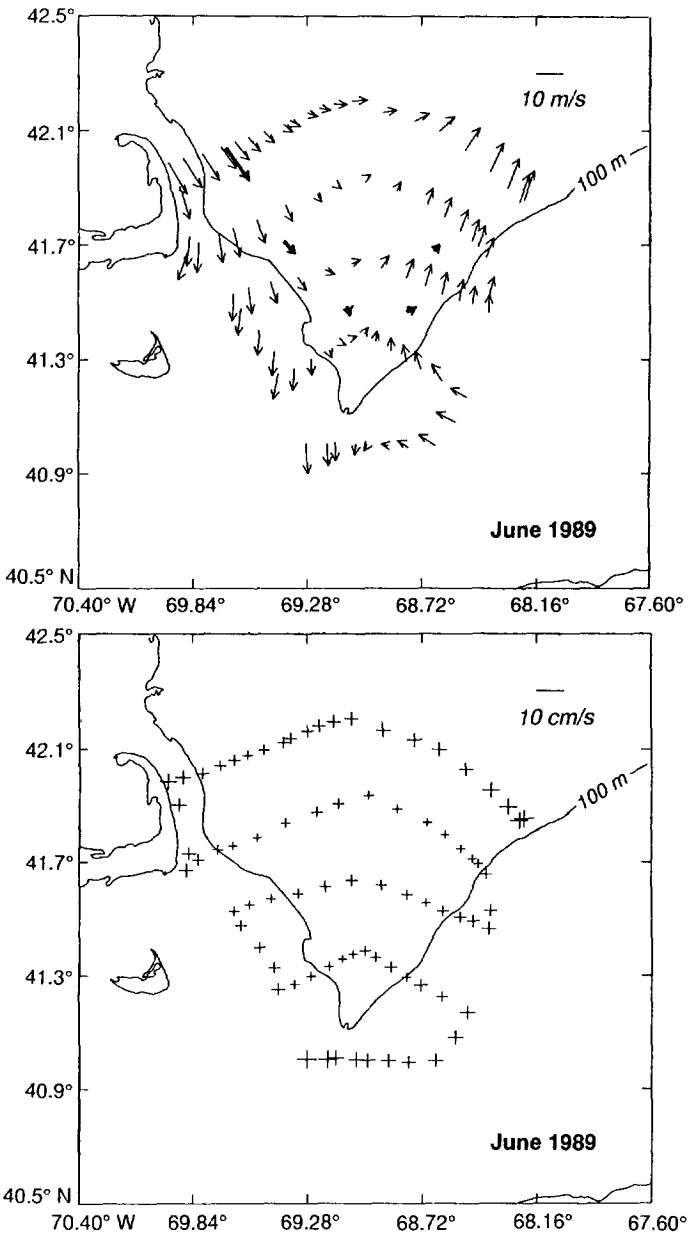

Fig. 5. Distributions of vertically averaged residual flow (upper) and fitting uncertainty (lower) in the northern GSC during the June 1989 CTD/ADCP survey. The plotting scale for the current vector and fitting uncertainty is shown in cm s^{-1} in the upper right of each panel. Also shown is the mean residual vertically averaged velocity (heavy solid arrow) measured during each of the small-scale biological surveys.

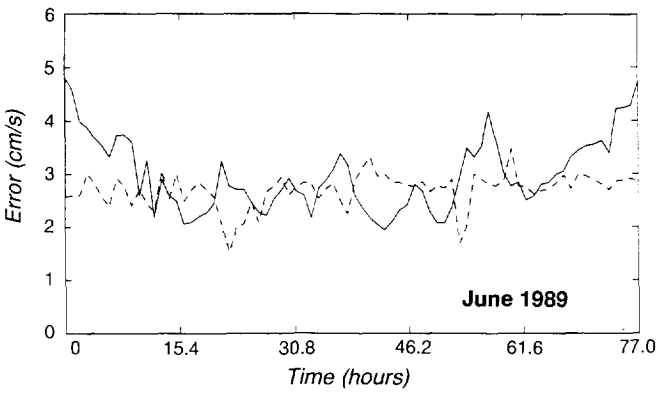

Fig. 6. Comparison between the fitting (solid line) and measurement (dashed line) errors along the ship's track during the 7–12 June 1989 CTD/ADCP survey.

was much stronger. While the fitting uncertainty is comparable or larger than the residual vectors in some regions in Figs 3–5, the spatial structure and strength of the residual current field are robust.

The magnitude of the fitting uncertainty was also compared with measurement error found using the vertically averaged ADCP data. As an example, the measurement error in the ADCP data from the June 1989 survey was reduced to $\pm$ 2–3 cm s^{-1} after vertically averaging for 1 h, which was comparable to the least-squares fitting uncertainty (Fig. 6). A spectral analysis of the time series of the fitting uncertainty showed that the energy of the unfitted error was distributed uniformly over the whole frequency domain. Since the measurement error was the same order of magnitude as the fitting uncertainty, no information about temporal variability of the residual flow can be resolved from the unfitted ADCP data.

Vertical structure of residual flow in the northern GSC

The residual currents were estimated with 4 m vertical resolution from 1-h-averaged ADCP data for the April 1988 and May–June 1989 SCOPEX surveys. *F*-tests showed a best fit for the residual flows with a second order polynomial for the April 1988 and June 1989 surveys, but a third order polynomial was required in the upper 100 m for the May 1989 survey. The standard deviations were inversely proportional to the degrees of freedom for fitting, and the correlations between raw and fitted residual flows were generally larger near the surface and bottom and smaller in mid-depths. For the June 1989 survey, the standard deviation was 2.0–3.0 cm s^{-1} in u and v at depths of 20–100 m where the correlation ranged from 0.85 to 0.95. The standard deviation increased to 5.0–7.0 cm s^{-1} near the surface due to a low correlation of about 0.50 in u and 0.75 in v and below 100 m due to a reduced number of degrees of freedom. Similar results were also found for the May 1989 survey: the standard deviation was about 1.5–3.5 cm s^{-1} in u and v in the upper 120 m where the correlation was about 0.70–0.80 in u and 0.9–0.95 in v, while the standard deviation was about 4.0–5.0 cm s^{-1} below 120 m where the numbers of acceptable quality ADCP data values were reduced and correlations became poor. However, relatively large

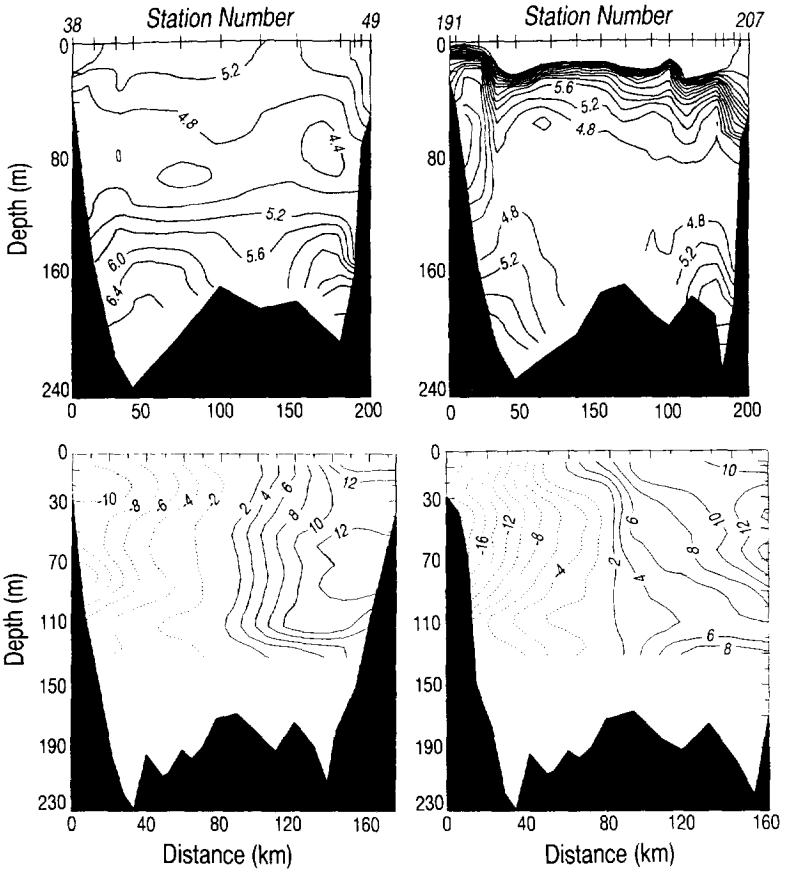

Fig. 7. Vertical sections of temperature (upper) and residual flow normal to temperature section (lower) on the northernmost transect (transect E) for April 1988 (left) and June 1989 (right) surveys. The velocity scale is in cm s^{-1}. A negative sign means flow into the northern GSC (southward) and a positive sign means flow out of the northern GSC (northward).

measurement noises caused low correlations and large deviations for the April 1988 survey, which were up to 7.0–8.0 cm s^{-1} at all measurement depths and the correlations were reduced to about 0.45, especially in the u component. Fitting uncertainty for the residual flow at a 95% confidence level was comparable to the standard deviation, even though there indeed existed a spatial distribution in fitting errors at each measurement depth. Therefore, the vertical structure of residual flow estimated from the April 1988 ADCP data is meaningful only in a qualitative rather than quantitative sense.

Vertical distributions of residual flow and water properties were consistent on hydrographic transects for both the April 1988 and June 1989 surveys (Fig. 7). In both surveys, the horizontal circulation is cyclonic-like at all levels throughout at least the upper 120 m, with maximum inflow and outflow occurring at the western and eastern ends of the transect. In April 1988, one inflow maximum occurred at a depth of 20 m, corresponding to the coastal-trapped low-salinity surface plume water found there (see Fig. 6 in CHEN *et al.*, 1995), and another inflow maximum and outflow were centered near 80 m in the core of

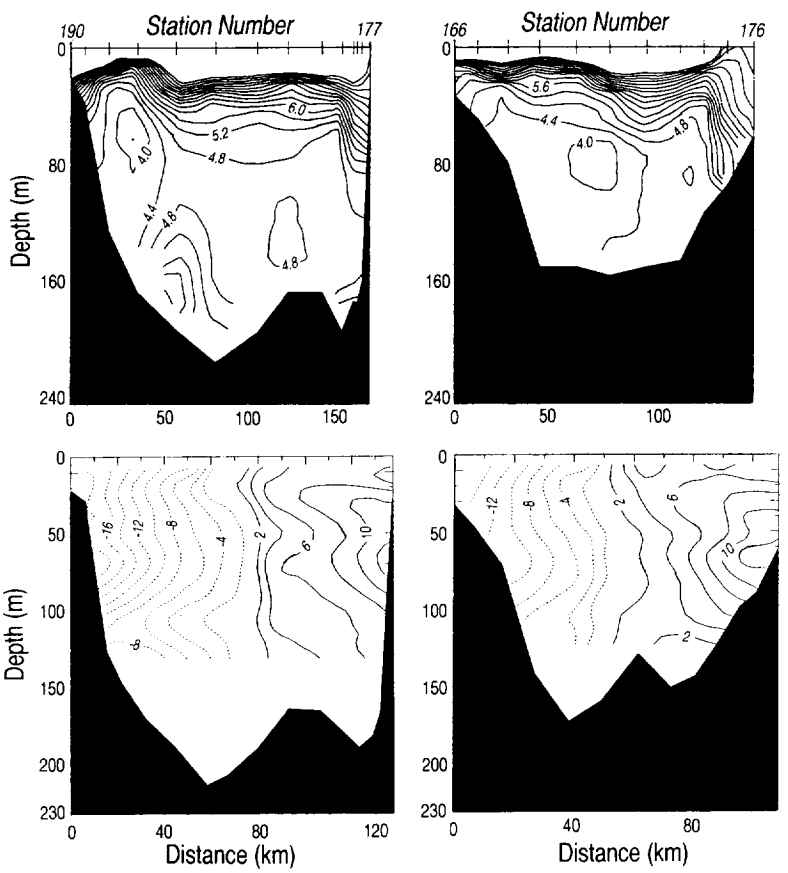

Fig. 8. (a) Vertical sections of temperature (upper) and residual flow normal to temperature section (lower) southward from transects D (left) and C (right) during the June 1989 survey. The velocity scale is in cm s^{-1}. A negative sign means flow into the northern GSC (southward) and a positive sign means flow out of the northern GSC (northward).

MIW denoted by a temperature minimum of about 4.4°C. Similarly, in June 1989, one inflow maximum was observed in the upper 20 m associated with the strong thermocline, and the other inflow maximum occurred in a broad band centered between 40 m and 70 m, which was also located in the center of MIW. Unlike April 1988, a narrow core of temperature minimum water with temperature range of 3.2° to 4.4° was observed during the June 1989 survey on the western flank over a horizontal distance of 40 km between 40 m and 120 m, which was distinct from the interior MIW. Corresponding to this subsurface core, a strong coastal jet-like flow was found over the western flank of the GSC at transect E, with a maximum velocity of about 18.0 cm s^{-1} at mid-depth and a strong horizontal shear of 10 cm s^{-1} over 40 km away from the coast.

The subsurface coastal jet-like flow observed in the June 1989 survey can be traced southward in subsequent sections D to B in Fig. 8, where the cold and relatively fresh water was carried into the northern GSC, flowing southward first along the 100-m isobath to mix with interior MIW and warm, saline Maine Bottom Water, and then turning northward to

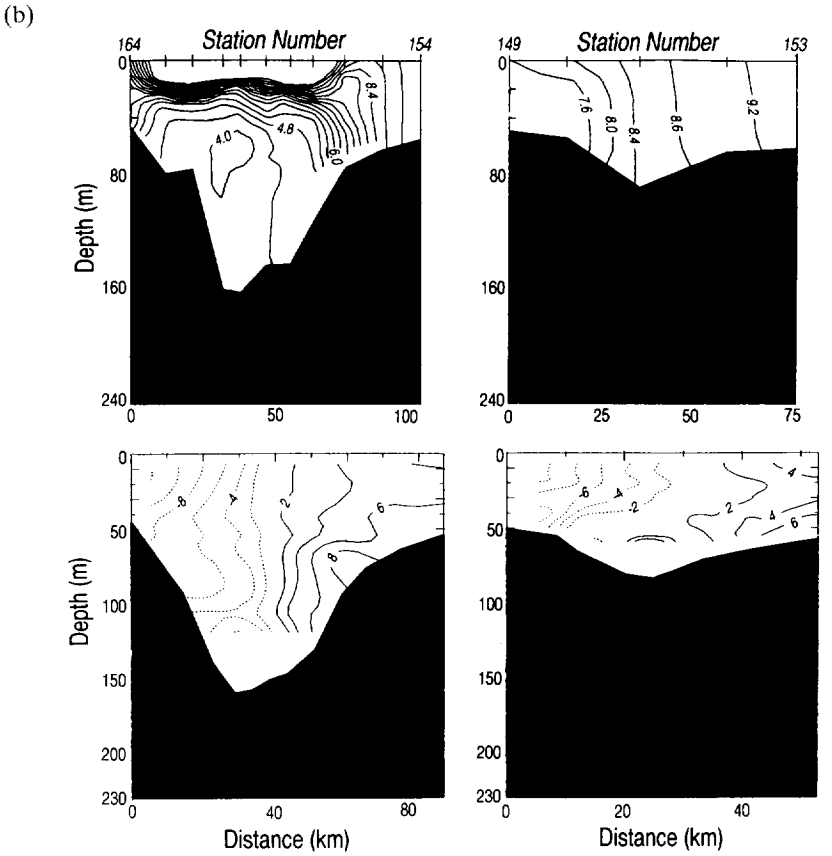

Fig. 8. (b) Vertical sections of temperature (upper) and residual flow normal to temperature section (lower) southward from transects B (left) and A (right) during the June 1989 survey. The velocity scale is in cm s^{-1}. A negative sign means flow into the northern GSC (southward) and a positive sign means flow out of the northern GSC (northward).

flow out of the northern GSC along the western flank of Georges Bank as MIW with a relatively weak temperature minimum. The strength of this deep current weakened southward. It decreased from 18.0 cm s^{-1} at transect E to 8.0 cm s^{-1} at transect B as it flowed along the western flank, and then increased again to 12.0 cm s^{-1} as it left the northern GSC along the western flank of Georges Bank, indicating that a large part of the deep MIW turned eastward as it flowed into the northern GSC and only a small portion of this water was carried southward to transect B. There did exist an outflow directly through the GSC from the western GOM on the western side of the southernmost transect A in the upper 50 m, consistent with *T–S* analysis (CHEN *et al.*, 1995). This implies that the southward outflow through the western GSC in the upper 50 m is a mixture of low-salinity surface plume water, Maine Surface Water, and a little MIW.

The seasonal intensification of the subsurface coastal jet-like current due to the increasing cooling and freshening was clearly identified through comparison between the

vertical structure of temperature and residual currents obtained in the May and June 1989 surveys. The narrow tongue of temperature minimum water, which was found in 7–12 June 1989, can be traced back to 19 and 21 May 1989, three weeks earlier, at the northernmost section but it was about 0.8°C warmer. Associated with this water mass, a relatively strong southward flow of order 12.0 cm s^{-1} was observed at the center of the temperature minimum, 6.0 cm s^{-1} weaker in strength than that observed in 7–12 June 1989 (for a detailed description, see CHEN, 1992).

Comparison with Lagrangian currents

During each regional survey, satellite-tracked drifters drogued at 5 and 50 m were deployed to measure Lagrangian movement of the near-surface water and sub-thermocline water, respectively (LIMEBURNER and BEARDSLEY, 1989).* The resulting low-passed trajectories taken from 28 April or 1 May to 31 May 1988, and from 11 to 30 June 1989 are plotted here in the upper panels of Figs 9 and 10, respectively, to show the spatial structure of the near-surface and 50 m water movement during these approximately 1-month periods.

In April–May 1988, while the near-surface Lagrangian flow looked very complex, especially in the central and northern GSC, some general tendencies can be identified. The mean movement of the near-surface water over the western flank of the GSC west of 69.0°W was southward, with some water flowing out of the GOM and onto the New England shelf. The near-surface water in the GSC, especially near and east of 69.0°W between 41.1°N and 41.6°N, tended to drift eastward and northeastward along the western and northern flank of Georges Bank. About 41.7°N, the near-surface water flowed northward and then turned northeastward to join the anticyclonic gyre along Georges Bank. The daily-averaged drifter speed varied from 0.1 to 16.0 cm s^{-1}, stronger over the shallower regions and weaker in the northern GSC between 41.3°N and 41.5°N. Similar daily mean trajectories of near-surface water were found in June 1989 where the low-passed Lagrangian flow followed three primary paths: (1) flow southward out of the GOM along the western flank of the GSC west of 69.0°W; (2) flow eastward and then northeastward from the central and northern GSC to the northern flank of Georges Bank; and (3) the anticyclonic circulation around Georges Bank. The daily-averaged drifter speed in June 1989 varied from 0.1 to 15.0 cm s^{-1}, with relatively weak flow in the center of the GSC between 41.3°N and 41.5°N.

The 50-m Lagrangian flow in the northern GSC during April–May 1988 and June 1989 was generally cyclonic from east of Cape Cod to the northern flank of Georges Bank. In April–May 1988, the daily-averaged 50-m drifter speeds varied from 0.5 to 5.0 cm s^{-1} in the western GSC where the local water depth was deeper than 100 m, but the drifter speeds increased to 15.0–20.0 cm s^{-1} as they drifted into the eastern GSC. In June 1989, the daily-averaged 50-m drifter speeds varied from 5 to 25 cm s^{-1} except in the center of the GSC and north of 42.0°N where the water speed was found to be 0.5–2.0 cm s^{-1}.

The residual flow field obtained at 7 and 51 m from the ADCP surveys in late April 1988 and mid-June 1989 are compared with the Lagrangian flow at 5 m and 50 m in Figs 9 and 10.

*Note: The drifters deployed in SCOPEX were the Argos-tracked, Low-Cost Drifters (LCD) manufactured by Draper Laboratory, Cambridge, Massachusetts. The drifters were deployed with holey-sock drogues centered at 5 or 50 m.

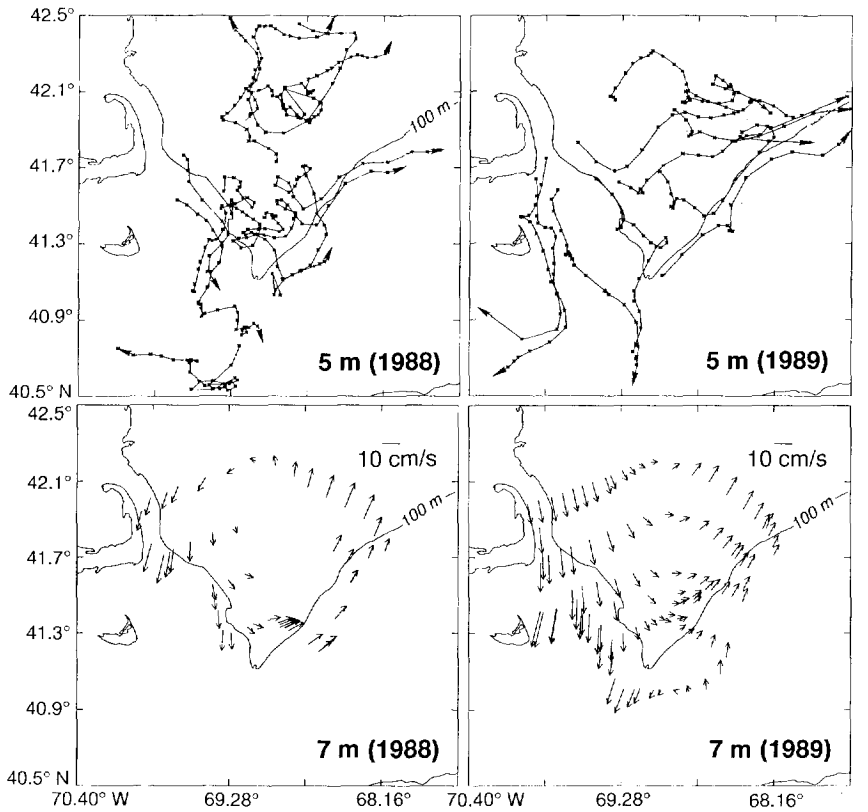

Fig. 9. Low-passed trajectories of 5-m drifters (upper) from 28 April or 1 May to 31 May 1988 and from 11 June to 30 June 1989, and maps of residual flow at 7 m (lower) in the northern GSC obtained during the April 1988 and June 1989 CTD/ADCP surveys. Direction of drifter displacement indicated by arrow placed at end of trajectory.

By definition, the Lagrangian velocity refers to the velocity of a fluid element which is dependent on position and time, while the Eulerian velocity is the velocity at a fixed point. If the flow field is steady, or, if the local derivatives of the flow are equal to zero, then the trajectory of a fluid element is equivalent to a streamline so that the Lagrangian velocity is equal to the Eulerian velocity at a fixed point. In both April–May 1988 and June 1989, however, the Lagrangian velocity data at 5 and 50 m started 1 or 2 days after the regional ADCP surveys were completed, so that it is difficult to compare quantitatively the Lagrangian velocity estimated from the drifter trajectories with the regional Eulerian velocity obtained from the ADCP data. In spite of this time mismatch and the questions associated with how well the drifters tracked water, the Eulerian flow field shows a reasonable agreement in direction and spatial structure with the mean paths of the drifters in April–May 1988 and June 1989, especially at mid-depth near 50 m. This horizontal structure is also seen in the 7-m and 51-m residual flow field in 19–21 May 1989 (Chen, 1992), suggesting that the flow pattern in the northern GSC during late spring is relatively stable in time, at least at mid-depth in the MIW.

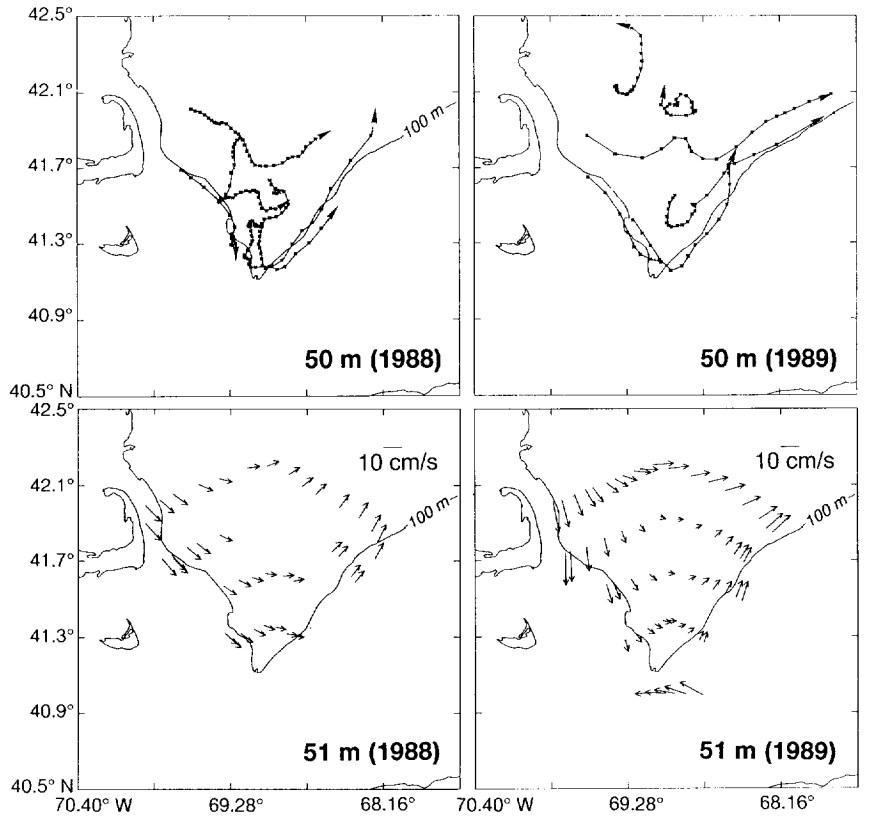

Fig. 10. Low-passed trajectories of 50-m drifters (upper) from 28 April or 1 May to 31 May 1988 and from 11 June to 30 June 1989, and maps of residual flow at 51 m (lower) in the northern GSC obtained during the April 1988 and June 1989 CTD/ADCP surveys. Direction of drifter displacement indicated by arrow placed at end of trajectory.

Discussion of possible driving forces

The vertical shear in the ADCP residual flow was qualitatively consistent with the vertical distribution of water density during the three SCOPEX regional surveys: the vertical shear was stronger near both ends of the CTD transects where the vertical gradient of water density was larger and weaker in the interior where the water density was almost vertically uniform (Fig. 7). This implies that the baroclinic motion in the northern GSC in late spring is controlled more by density forcing than tidal rectification. The relative importance of density forcing and tidal rectification to the residual flow in the northern GSC can be estimated by comparison between the vertically-averaged ADCP residual flow and the tidally rectified flow predicted numerically by GREENBERG (1983) and LYNCH and NAIMIE (1993) and comparison between the ADCP residual flow and geostrophic shears. Over the western flank of the GSC east of Cape Cod where the water depth is shallower than 60 m, the numerical models predict a southward tidally rectified current of 7–10 cm s^{-1}, about the same order of magnitude as the ADCP mean current, while the geostrophic shear is almost equal to zero since the water was vertically well-mixed there.

Table 1. *Southward Transports of the Low-Salinity Plume (LSP) and MIW*

Survey time	Transport	
	LSP (Sv)	MIW (Sv)
April 1988	-0.07 ± 0.03	-0.31 ± 0.38
June 1989	-0.12 ± 0.06	-0.66 ± 0.14

Over the sloping western and eastern flanks of the GSC where the water depth is between 60 and 200 m, the predicted tidally rectified current is about 0.1–1.0 cm s^{-1}, only about 1–10% of the ADCP residual current, while the geostrophic shear can reach 0.4×10^{-2} s^{-1}, which was comparable in magnitude to the ADCP residual shear. In the central region of the northern GSC, the tidally rectified flow is only about 0.1 cm s^{-1}, and the geostrophic shear associated with MIW was almost zero within the MIW where water properties were almost spatially uniform. Therefore, we conclude that the water motion in late spring is driven primarily by density forcing over the slope and deeper part of the northern GSC and more by tidal rectification over the shallower sides of the northern GSC. Moreover, the vertical uniform flow associated with the MIW in the central region of the GSC is probably controlled by the local bottom topography with an influence of deep MBW.

4. SOUTHWARD TRANSPORTS OF THE LOW-SALINITY PLUME AND MIW

It is difficult to estimate the total mass transport across different sections using the SCOPEX CTD/ADCP measurements because the ADCP profiler could not resolve currents below 140 m. Brooks (1990) deployed three current meters at Lindenkohl Sill between Georges Basin and Wilkinson Basin in June 1986. The resulting low-frequency current near the bottom showed a good correlation with the surface wind when the density stratification was relatively weak but they were decoupled when density stratification became stronger. A strong current of order 100 cm s^{-1} was found near the bottom during wind-coherent intervals, while currents were intensified at mid-depth and upper level during wind-current decoupled intervals. This suggests that MBW may contribute a large part of the total mass transport in the deeper areas of the northern GSC. For this reason, we focus our study here only on transports of the near-surface low-salinity plume and MIW.

Transports of the low-salinity plume and MIW across the northernmost transect (transect E) were different for the April 1988 and June 1989 surveys (Table 1). In April 1988, the low-salinity plume was identified by a strong salinity front of 32.5 on the western flank of the northern GSC, with a maximum depth of about 40 m and a cross-shelf scale of about 40 km. The southward volume transport of this plume was about 0.07 ± 0.03 Sv with a mean salinity of 32.2. In June 1989, the low-salinity plume as defined by the 32.5 isohaline was much fresher and occupied a large area of the northern GSC. The southward volume transport of the plume was increased to 0.12 ± 0.06 Sv with a mean salinity of 31.4, almost twice as large as that in April 1988. As noted before, the difference in the transport of the low-salinity plume between these two years is mainly due to the increased freshwater river discharge in late spring 1989.

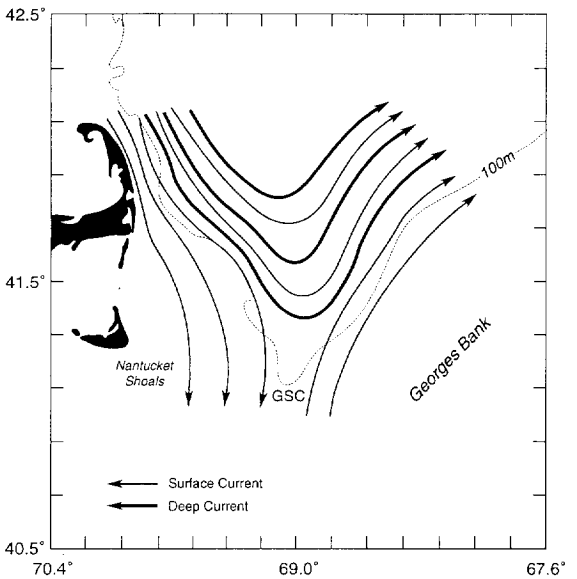

Fig. 11. Conceptual model of the upper and lower layer circulation in the northern GSC during late spring. The map is made according to the residual current structure deduced from the detided April 1988 and May–June 1989 ADCP measurements and the low-passed trajectories of satellite-tracked drifters deployed at 5 and 50 m.

The transport of MIW was estimated from the flow of water with $T \leq 4.8°$ located between 40 and 120 m depths. There was a big difference in the southward transport between the April 1988 and June 1989 surveys. The southward transport of MIW was about 0.31 ± 0.38 Sv in April 1988, while it increased to -0.66 ± 0.14 Sv in June 1989. The larger southward transport of MIW in June 1989 was due to the existence of the strong coastal jet flow over the western flank of the northern GSC. There was also a big difference in the net flux of MIW across the northern GSC between these two surveys. In April 1988, the net flux across section E was northward, with a transport of 0.73 ± 0.47 Sv, while in June 1989 it was southward, with a transport of 0.02 ± 0.06 Sv. The large northward transport found in the upper 120 m in April 1988 suggests an intrusion of the anticyclonic Georges Bank circulation into the northern GSC during the measurement time since part of the water in the eastern side of the GSC was different from that in the western side of the GSC and can be traced back to Georges Bank. A strong southward wind higher than 15 m s^{-1}, recorded just before the April 1988 survey, may have caused the westward shift of the anticyclonic gyre around Georges Bank, and hence increased the northward transport on the eastern side of the northern GSC. The small net southward transport found in June 1989 suggests that most of the MIW was recirculated cyclonically along the local isobaths and only a small amount of MIW flowed southward through the GSC onto the outer shelf. This result is consistent with the T–S analysis presented in CHEN *et al.* (1995).

5. DISCUSSION AND CONCLUSIONS

The residual flows computed from detided ADCP data collected in late spring of 1988 and 1989 clearly show different circulation patterns near-surface and deeper (Fig. 11). In

the upper 50 m, the residual flow in the northern GSC consists of three principal currents: (1) a southward coastal current along the western flank of the GSC; (2) a broad cyclonic circulation along the local topography in the interior region of the GSC; and (3) the northeastward current around Georges Bank. Below 50 m, the residual current tended to flow cyclonically along the local 100-m isobath across the northern GSC. Associated with these circulation patterns were two velocity maxima in the vertical: one was near the surface to drive the surface water, the other was at mid-depth to carry MIW into and through the northern GSC region. The residual ADCP current patterns are consistent with the vertical distributions of water masses and the trajectories of satellite-tracked drifters drogued at 5 and 50 m in the GSC.

Significant differences were found in the vertical structure of the residual flow and associated southward transport of the low-salinity plume and MIW between April 1988 and June 1989. A cool and fresh (hence light) coastal jet-like current was found at mid-depth of the northern GSC in May and June 1989 but not in April 1988. The southward transports of low-salinity plume water and MIW in April 1988 were about 0.07 ± 0.03 Sv and 0.31 ± 0.38 Sv, respectively, while in June 1989, they increased to about 0.12 ± 0.06 Sv and 0.66 ± 0.14 Sv, respectively. The larger transports of low-salinity plume water and MIW found in June 1989 are believed to be due to the increased freshwater river discharge and occurrence of the deep coastal jet along the western flank of the GSC.

Comparisons between the ADCP residual and geostrophic current shears and between the ADCP residual and numerically predicted tidal-rectified currents suggest that the residual current in late spring is mainly driven by tidal rectification over the shallower sides of the GSC and by buoyancy forcing over the deeper flanks and in the central region of the GSC.

Acknowledgements—This research was supported by the National Science Foundation under grants OCE 87-13988 and OCE 91-01034. We would like to thank Ken Brink, Julio Candela, Dave Chapman, Glenn Flierl, Glen Gawarkiewicz, Steve Lentz and Paola Rizzoli for their interest in this work and valuable comments and suggestions. We also wanted to thank Graham Giese, Karen Wishner and Howard Winn, who provided us tidal gauge, zooplankton concentration and whale-sighting data.

REFERENCES

Beardsley R. C., C. S. Chen, K. Wishner and M. Macaulay (1990) Spatial variability in stratification and zooplankton distribution near feeding right whales in the Great South Channel. *EOS, Transactions of the American Geophysical Union*, **71**(2), 68.

Bigelow H. B. (1927) Physical oceanography of the Gulf of Maine. *Bulletin of the U.S. Commerce Bureau*, **40**, 511–1027.

Brooks D. A. (1990) Currents at Lindenkohl Sill in the southern Gulf of Maine. *Journal of Geophysical Research*, **95**(C12), 22,173–22,192.

Brownlee K. A. (1965) *Statistical theory and methodology in science and engineering*. J. Wiley and Sons, New York, 590 pp.

Butman B., J. W. Loder and R. C. Beardsley (1987) The seasonal mean circulation: observation and theory. In: *Georges Bank*, R. H. Backus, editor, the MIT press, Cambridge, Massachusetts, pp. 125–135.

Candela J., R. C. Beardsley and R. Limeburner (1992) Separation of tidal and subtidal currents in ship-mounted Acoustic Doppler Current Profiler observations. *Journal of Geophysical Research*, **97**(C1), 769–788.

Cetacean and Turtle Assessment Program (CETAP) (1982) *A characterization of marine mammals and turtles in the Mid- and North Atlantic areas of the U.S. outer continental shelf, Final Report*. Contract No. AA551-CT8-48. Bureau of Land Management, U.S. Department of Interior, Washington, D.C., 586 pp.

CHELTON D. B. (1982) Statistical reliability and the seasonal cycle: comments on "Bottom pressure measurements across the Antarctic Circumpolar Current and their relation to the wind." *Deep-Sea Research*, **29**, 1381–1388.

CHEN C. (1992) Variability of currents in Great South Channel and over Georges Bank: observation and modeling. Ph.D. Thesis, MIT/WHOI Joint Program, Woods Hole, Massachusetts, WHOI-92-20, 283 pp.

CHEN C. (1989) The structure of the Kuroshio west of Kyushu. M.S. Thesis, MIT/WHOI Joint Program, Woods Hole, Massachusetts, 137 pp.

CHEN C., R. C. BEARDSLEY and R. LIMEBURNER (1995) Variability of water properties in late spring in the northern Great South Channel. *Continental Shelf Research*, **15**, 415–431.

DRAPER N. R. and H. SMITH (1966) *Applied regression analysis*. J. Wiley and Sons, New York, 407 pp.

FOFONOFF N. P. and H. BRYDEN (1975) Specific gravity and density of seawater at atmospheric pressure. *Journal of Marine Research*, **33**(Supplement), 69–82.

FREELAND H. J. and M. G. G. FOREMAN (1990) Tide removal from ship-mounted Doppler measurements. *EOS, Transactions of the American Geophysical Union*, **71**(2), 74.

GEYER R. and R. SIGNELL (1990) Tidal flow measurements around a headland with a shipboard Acoustic Doppler Current Profiler. *Journal of Geophysical Research*, **95**, 3189–3197.

GREENBERG D. A. (1983) Modeling the mean barotropic circulation in the Bay of Fundy and Gulf of Maine. *Journal of Physical Oceanography*, **13**, 886–904.

JOYCE T. M. (1989) On *in-situ* "calibration" of shipboard ADCPs. *Journal of Atmospheric and Oceanic Technology*, **6**, 169–172.

LIMEBURNER R. and R. C. BEARDSLEY (1989) Lagrangian circulation in the Great South Channel and on Georges Bank during summer. In: *Proceedings of Third Georges Bank Research Workshop*, Bedford Institute of Oceanography, 29 pp.

LODER J. W., D. BRICKMAN and P. W. HORNE (1992) Detailed structure of currents and hydrography on the northern side of Georges Bank. *Journal of Geophysical Research*, **97**, 14,331–14,352.

LWIZA K. M. M. and D. G. BOWERS (1990) Measurements of tidal and residual currents at a front in the North Sea using an acoustic Doppler current profiler. *EOS, Transactions of the American Geophysical Union*, **71**(2), 149.

LYNCH, D. R. and C. E. NAIMIE (1993) The M_2 tide and its residual on the outer banks of the Gulf of Maine. *Journal of Physical Oceanography*, **23**(10), 2222–2253.

MOODY J. A., B. BUTMAN, R. C. BEARDSLEY, W. S. BROWN, P. DAIFUKU, J. D. IRISH, D. A. MAYER, H. O. MOFJELD, B. PETRIE, S. RAMP, P. SMITH and W. R. WRIGHT (1984) Atlas of tidal elevation and current observations on the northeast American continental shelf and slope. *U.S. Geological Survey Bulletin*, **1611**, 122 pp.

WISHNER K. and J. SCHOENHERR (1992) Spatial and temporal variability of copepod (*Calanus finmarchicus*) distribution during the spring in the southern Gulf of Maine. In: *Proceedings of the Gulf of Maine Scientific Workshop, Woods Hole, MA*, 8–10 January 1991, J. WIGGIN and C. N. K. MOOERS, editors, Gulf of Maine Council on the Marine Environment, Urban Harbors Institute, University of Massachusetts, Boston, pp. 296–298.

WISHNER K., J. SCHOENHERR, R. BEARDSLEY and C. CHEN (1995) Abundance, distribution and population structure of the copepod *Calanus finmarchicus* in a springtime right whale feeding area in the southwestern Gulf of Maine. *Continental Shelf Research*, **15**, 475–507.

APPENDIX

The multiple least-squares regression method to fit the raw ADCP data is briefly described next (BROWNLEE, 1965; DRAPER and SMITH, 1966; FOFONOFF and BRYDEN, 1975). Given data for Y_n for u_n or v_n; (where $n = 1, 2, 3, \ldots, N$), the regression formula (2.1) of r degrees of the polynomials for total low-frequency and tidal currents can be simply rewritten as

$$\hat{Y}_n = \sum_{i=1}^{r} a_i X_{ni}, \tag{A.1}$$

where $\hat{Y}_n$ is the predicted value for Y_n. X_{ni} is an independent variable consisting of the different terms of the polynomials or products of the polynomials with the periodic functions prescribed by the known tidal frequencies. The least-squares estimates for a_i can be obtained subject to minimization of the square residuals

$$G_{Nr} = \sum_{n=1}^{N} (Y_n - \hat{Y}_n)^2. \tag{A.2}$$

Minimization of G_{Nr} with respect to a_i yields the normal equations in the matrix form

$$(\mathbf{X}'\,\mathbf{X})\,\mathbf{A} = \mathbf{Y}, \tag{A.3}$$

where $\mathbf{X} = \{X_{ni}\}$, $\mathbf{A} = \{a_i\}$ and $\mathbf{Y} = \{\Sigma_{n=1}^{N} X_{ni} Y_n\}$. The prime $'$ denotes the transpose of the matrix. Let $\mathbf{C}$ be the inverse of matrix $(\mathbf{X}'\,\mathbf{X})$, then

$$\mathbf{A} = \mathbf{C}\,\mathbf{Y}. \tag{A.4}$$

If Y_n is assumed to be a random variable normally distributed about a true value with variance σ^2, the coefficients a_i will also be random variables with variance given by

$$\sigma_{a_i}^2 = C_{ii}\sigma^2, \tag{A.5}$$

and the unbiased expected value for σ^2 is

$$\sigma^2 = \frac{G_{Nr}}{(N-r)}, \tag{A.6}$$

where $(N - r)$ is the degrees of freedom for the least-squares regression.

Two statistical tests using the student's t-distribution and the F-distribution have been made to test if each a_i is significantly different from zero at the 95% confidence level and if adding higher order polynomials into the regression gives a significantly better fit. For a normal distribution, the ratio $a_i/\sigma\sqrt{C_{ii}}$ satisfies a student's t-distribution with $N - r$ degrees of freedom. Therefore, a_i become significantly different from zero at a 95% confidence level only if

$$\left|\frac{a_i}{\sigma\sqrt{C_{ii}}}\right| > t_{0.05}(N-r). \tag{A.7}$$

A higher order of polynomial is important only if it significantly reduces the square residual for fitting. For a normal distribution, the ratio $(G_{Nq} - G_{Nr})/(q - r)\sigma_q$ has an F-distribution with $q - r$ degrees of freedom for the first fit and $N - 1 - r$ degrees of freedom for the second fit. At a 95% confidence level, additional terms $(q - r)$ are significant only if

$$\frac{G_{Nr} - G_{Nq}}{(q-r)\sigma_q} > F_{0.05}(q-r, N-1-r). \tag{A.8}$$

The uncertainty in the predicted value $\hat{Y}_n$ from the true value Y_n is given by the standard deviation of $\hat{Y}_n$, which is equal to

$$\sigma_{\hat{Y}_n} = \sigma\sqrt{\mathbf{X}_n'\,\mathbf{C}\,\mathbf{X}_n}. \tag{A.9}$$

At a 95% confidence limit ($\alpha = 0.05$) on the true mean value of Y_n at $\mathbf{X}_n$, the fitting error of the least-squares regression at position $\mathbf{X}_n$ is given by

$$\Delta Y_n = \pm t\{(N-r-1), 1 - \tfrac{1}{2}\alpha\}\sigma\sqrt{\mathbf{X}_n'\,\mathbf{C}\,\mathbf{X}_n}, \tag{A.10}$$

which is a function of position (x, y) and degrees of freedom $(N - r - 1)$.